International Journal of Engineering & Technology, 7 (4.26) (2018) 1-5

International Journal of Engineering & Technology

Website: www.sciencepubco.com/index.php/IJET

Research paper



Correlation of Biomechanical Properties and Grayscale of Articular Cartilage using Low-Field Magnetic Resonance Imaging

Yew Wansin[1], Mohd Juzaila Abd Latif [1,2]*, Sharifah Majedah Idrus Alhabshi[3], Jamaluddin Mahmud[4], Mohammed Rafiq Abdul Kadir[5]

[1]*Fakulti Kejuruteraan Mekanikal, Universiti Teknikal Malaysia Melaka, Hang Tuah Jaya 76100 Durian Tunggal, Melaka, Malaysia.*
[2]*Centre for Advanced Research on Energy (CARe), Universiti Teknikal Malaysia Melaka, Hang Tuah Jaya 76100 Durian Tunggal, Melaka, Malaysia.*
[3]*Department of Radiology, Faculty of Medicine, Universiti Kebangsaan Malaysia Medical Centre, 56000 Cheras, Kuala Lumpur, Malaysia.*
[4]*Faculty of Mechanical Engineering, Universiti Teknologi MARA, 40450 Shah Alam, Selangor, Malaysia.*
[5]*Faculty of Engineering, Universiti Teknologi Malaysia, 81310 Skudai, Johor, Malaysia.*
**Corresponding author E-mail: juzaila@utem.edu.my*

Abstract

Osteoarthritis is a joint disease that caused by the progression of degenerative articular cartilage tissue. The degeneration of the articular cartilage resulted in alteration of the biomechanical properties. Magnetic resonance imaging (MRI) has become the most potential imaging technique to assess the condition of the articular cartilage. However, most of the previous studies of articular cartilage were performed using high-field MRI units. Therefore, this study aimed to examine the correlation between the biomechanical properties of articular cartilage and the image grayscale using low-field MRI. Cartilage specimens extracted from bovine femoral head were scanned using 0.2 T MRI to obtain the cartilage image. The MRI image was characterized based on the intensity of grayscale. Indentation test was then conducted on the specimen to characterize the cartilage biphasic properties of elastic modulus and permeability. The cartilage grayscale values were moderately correlated with cartilage biphasic elastic modulus and higher correlation was observed with the permeability. These could indicate the potential application of low-field MRI to evaluate the biomechanical properties of articular cartilage.

Keywords: *Articular cartilage; low-field magnetic resonance imaging; image grayscale; elastic modulus; permeability.*

1. Introduction

Osteoarthritis (OA) is a joint disease caused by the progression of degeneration of the articular cartilage tissue in human body. OA is also characterized by joint pain, reduced joint movement, cartilage loss, subchondral bone changes, and synovial infection [1-3]. Early detection of OA is a great interest to orthopedics surgeons, rheumatologists, radiologists, and researchers because it allows early intervention and treatment.

The ability of articular cartilage to perform its physiological functions depends on the structure, the composition and the integrity of its extracellular matrix (ECM) as the matrix generates the tensile and compressive stiffness of the cartilage [4,5]. Alteration of biomechanical properties due to loss of proteoglycan and increase in water content occur before the structural alterations in cartilage tissues [2]. The structural changes of cartilage could be validated by the cartilage biphasic biomechanical properties [6]. Elastic modulus and permeability are important properties to represent the biphasic properties of solid and fluid phases of cartilage.

Although there are various methods used to examine and diagnose the OA disease, magnetic resonance imaging (MRI) has received much attention as a premier non-invasive imaging technique because it provides excellent image of soft tissue especially articular cartilage [6,7]. The strength of the magnetic field contributes to the strength of the signal used to generate images. The MRI scanner can be generally categorized based on its magnetic strength as low (<1.5 T), high (1.5-7.0 T), and ultra-high (>7.0 T). Most of the studies were conducted using high-field MRI scanner to examine articular cartilage properties since these MRI scanners were clinically used to diagnose patients [2,8-10]. However, the purchase and maintenance costs of the high-field MRI was much higher as compared with the low-field MRI [11,12]. It was reported that although the high-field MRI provides better quality images, comparable image evaluations of the cartilage were found using the low-field MRI [7,13,14].

In previous studies, the low-field MRI has been utilized to quantify the morphology of the articular cartilage and to determine the bone erosions or cartilage lesions [14-17]. However, further abilities of the low-field MRI to study the articular cartilage are yet to be explored. Therefore, the objective of this study is to determine the correlation of the biomechanical properties of articular cartilage and the image grayscale generated from the low-field MRI. The outcome of this study could be used to give an insight of the other potential used of low-field MRI to monitor and examine the condition of articular cartilage.

Copyright © 2018 Authors. This is an open access article distributed under the Creative Commons Attribution License, which permits unrestricted use, distribution, and reproduction in any medium, provided the original work is properly cited.

2. Methodology

2.1. Specimen Preparation

Fresh articular cartilage of five femoral heads were harvested from bovine hip joint aged between 3 to 4 years old obtained from a local abattoir within 24 hours of death. The femoral head was then cut into sagittal and transverse sections to yield four cartilage specimens labelled as lateral left (LL), lateral right (LR), medial left (ML) and medial right (MR) as shown in Figure 1. During the specimen preparation, the cartilage specimens (n=20) were regularly washed with phosphate buffered saline to keep the cartilage hydrated. The specimens were then stored at 7℃ in moist conditions within 48 hours prior experimental testing and MRI scanning.

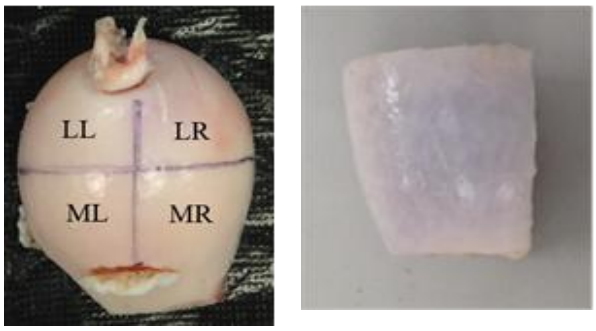

(a) (b)

Fig. 1: Articular cartilage (a) femoral head, (b) cartilage specimen.

2.2. Magnetic Resonance Imaging

The specimens were scanned using low-field 0.2 T Esaote C-scan MRI system (Genova, Italy). Three standard imaging sequences available in the system were utilized in order to select sequence that can produce the best quality image of the cartilage from the MRI system. The imaging sequences are gradient echo, spin echo and turbo 3D sequences where the imaging parameters are shown in Table 1. During the scanning, the specimen was immersed in PBS.

Table 1: The acquisition parameters of the MRI sequences.

Sequence	Repetition time (TR), ms	Echo time (TE), ms	Matrix size	Field of view (FOV), mm
Gradient echo	780	10	256 × 256	100
Spin echo	800	18	256 × 256	100
Turbo 3D	50	16	192 × 192	180

2.3. Grayscale Characterization of MRI Image

The cartilage image was characterized based on the image grayscale at the region of interest (ROI) of 10 × 2 pixel matrix located at the center point of the cartilage specimen as shown in Figure 2. The grayscale at the center point of the cartilage specimen was only considered because the indentation test was performed at the particular point to obtain the biomechnical properties. The grayscale values were determined using MATLAB software (MathWorks Inc., MA, USA).

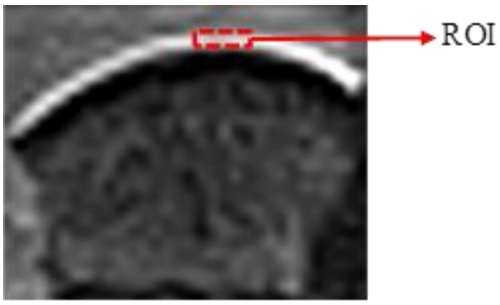

Fig. 2: MRI image of articular cartilage specimen.

2.4. Characterization of Biomechanical Properties

The biomechanical properties of the cartilage were characterized using a combination of experimental and computational methods which was used in previous studies [18,19]. Creep experiment tests were performed using a customized indentation apparatus as shown in Figure 3. The creep indentation test was conducted at the center point of each cartilage specimen where the grayscale of the MRI image was determined. The test was performed using a 4 mm diameter spherical indenter subjected to 0.38 N load for 1000 s where the displacement of the cartilage had reached equilibrium and resulted 15% to 35% of cartilage deformation. The displacement was monitored using linear variable differential transformer (LVDT) and recorded every 0.01 s using LabVIEW software (National Instruments Corp., Austin, TX, USA).

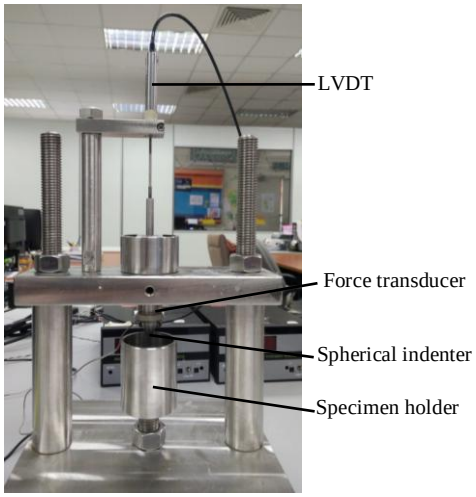

Fig. 3: Apparatus for indentation test rig.

The thickness of the cartilage was measured to develop specimen-specific finite element model. It was measured using a sharp needle indenter with 3.16 N compression load where the needle penetrated the cartilage until it reached the underlying bone. In order to establish more accurate contact load, the displacement and load of the indenter were recorded every 0.001 s. The thickness was obtained by determining the position of the needle indenter from the cartilage surface to the subchondral bone as described previously [20].

Linear axisymmetric biphasic finite element (FE) models of articular cartilage and subchondral bone were then developed based on the measured thickness and surface radius of each specimen using Abaqus software (DS Simulia Corp., Providence, RI, USA) as shown in Figure 4. The cartilage was modelled as biphasic material using four-node bilinear displacement and pore pressure elements (CAX4P) and the subchondral bone was modelled using four-node bilinear elements (CAX4) with elastic modulus of 2000 MPa and Poisson's ratio of 0.2 [19,20]. The spherical indenter was modelled as an analytical rigid body. The boundary and interface conditions were applied on the FE modelling to simulate the experimental creep indentation test such that the nodes on the axis were constrained in the horizontal direction, whilst the bottom nodes of the bone were constrained in both horizontal and vertical directions. The spherical indenter was only allowed to move in the vertical direction. The verification of the FE model was performed and described previously [20].

These FE models were used to determine the biphasic cartilage properties of elastic modulus and permeability as described previously by Hashim et al. (2017). The values of the two parameters were iteratively altered until the deformation-time curve generated from the FE model matched the creep indentation test. The curve-fitting was achieved using a nonlinear least-squares method using Matlab (V7.12.0 R2011a, MathWorks Inc, MA, USA) following the method developed by Pawaskar et al. (2010).

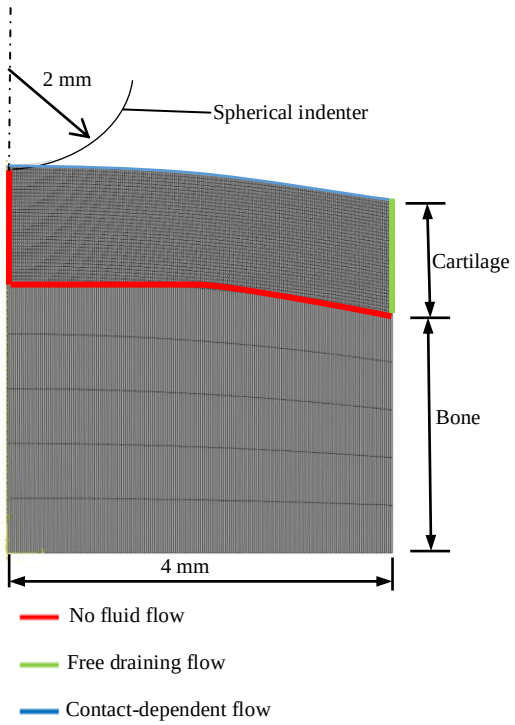

Fig. 4: Axisymmetric FE model of the cartilage specimen.

2.5. Correlation of MRI Image Grayscale and Biomechanical Properties

The correlation between the cartilage grayscale obtained from the MRI images and the biomechanical properties of each cartilage specimen was examined using the linear Pearson correlation method.

3. Result and Discussion

3.1. MRI sequence

Selection of the imaging sequence for the cartilage is crucial because it could give better contrast in cartilage compared to the surrounding tissues. Figure 5 shows the images produced from three different imaging sequences. It was observed that the gradient echo and spin echo sequences could differentiate the distinct region of the cartilage compared to the turbo 3D sequence. Moreover, the thickness of the cartilage measured from the image produced by the gradient echo and spin echo sequences were similar to the experiment result.

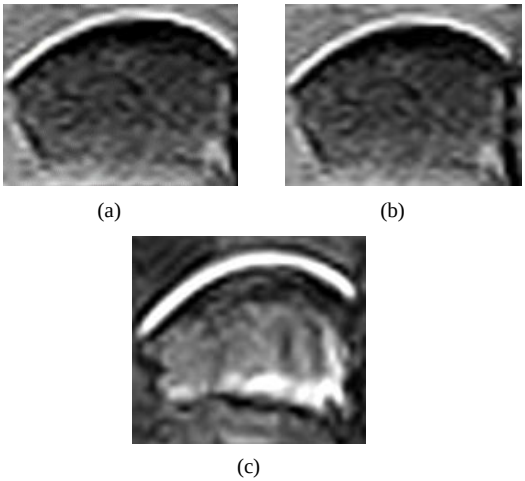

(a) (b)

(c)

Fig. 5: MRI images from different imaging sequences: (a) Gradient Echo; (b) Spin Echo; (c) Turbo 3D.

The average grayscale value obtained from the spin echo and gradient echo sequence were 764.15 ± 165.86 and 1396.95 ± 245.79 respectively. Based on the standard deviation, the gradient echo could provide higher sensitivity of grayscale value for the cartilage. This sequence was also applied in previous studies to examine the water distribution in cartilage and detect cartilage lesions using low-field MRI unit [12,14,16,17,21,22].

3.2. Biomechanical Properties

The average value of elastic modulus and permeability of the cartilage were 1.16 ± 0.89 MPa and 0.66 ± 0.50 $\times 10^{-15}$ m^4/Ns respectively, which are within the range determined from the previous studies using bovine femerol head [23,24]. The characterized biomechanical properties of the cartilage specimens for every quadrant are shown in Figure 6. It was observed that the properties vary between the quadrants where the elastic modulus was found between 1.05 ± 0.88 MPa to 1.33 ± 0.42 MPa, and the permeability was between 0.36 ± 0.10 $\times 10^{-15}$ m^4/Ns to 0.93 ± 0.70 $\times 10^{-15}$ m^4/Ns. The inhomogeneity of biomechanical properties across the articular cartilage in synovial joint were also found in previous studies [25,26]. This is due to the natural remodelling of the cartilage to withstand altered stresses during normal physiologic loading [27].

3.3. MRI Image Grayscale

In the present study, there were only two layers of pixel obtained in the cartilage region since the plane resolution of the image was 0.39 mm and the average measured thickness was 1.13 ± 0.07 mm. These two layers could represent the superficial/middle zone and deep zone of the cartilage which contains different composition and structure in the cartilage tissue where the average grayscale was found to be 1342.29 ± 219.96 and 1203.75 ± 237.07 respectively as shown in Figure 7.

The grayscale of the superficial zone was 10% higher compared to the deep zone. This could be due to the water content where studies have shown that higher water content was found in superficial and middle zones compared to the deep zone in cartilage [28,29]. Similar trend was also observed using high-field MRI between the grayscale stratification and the zones in the cartilage where higher signal intensity at the superficial zone was generated compared to the zone closer to the tidemark and subchondral bone for normal cartilage [30,31]. This could indicate that the low-field MRI have the potential to evaluate different physiological characteristics throughout the thickness of the articular cartilage using the image grayscale.

3.4. Correlation of Image Grayscale and Biomechanical Properties

Linear correlation analysis was performed to examine the relationship between the grayscale and biomechanical properties of articular cartilage, as shown in Figure 8. Elastic modulus increased linearly with increasing grayscale value in moderate relationship (r = 0.568). Meanwhile, the similar trend in permeability was observed and higher correlation (r = 0.632) was found between the permeability and the grayscale.

In previous studies, correlation between MRI parameters and biomechanical properties of articular cartilage were carried out using either high-field or ultra-high MRI where the correlation results were varies from 0.5 to 0.8 [23,32]. Comparable results were observed in the present study which indicate the potential used of low-field MRI to provide important information to evaluate and monitor the cartilage. Further studies are required to utilize the image grayscale values from low-field MRI to examine the condition of articular cartilage.

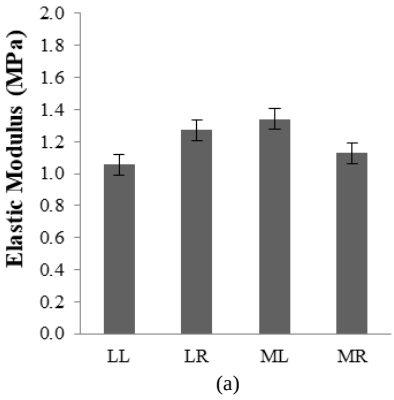

(a)

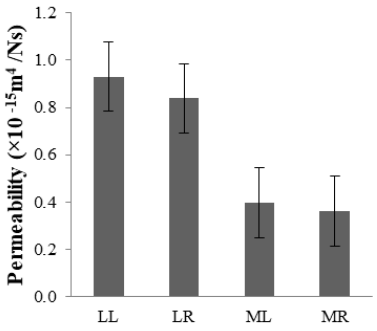

(b)

Fig. 6: Biphasic biomechanical properties of cartilage at four different quadrants (a) elastic modulus (b) permeability.

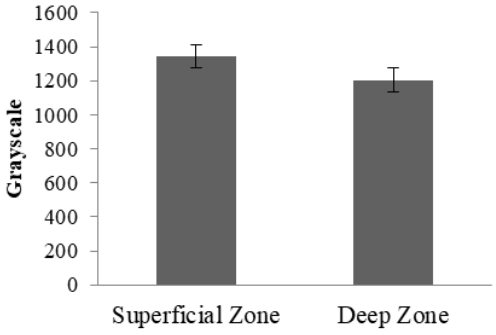

Fig. 7: Cartilage grayscale of the superficial and deep zones.

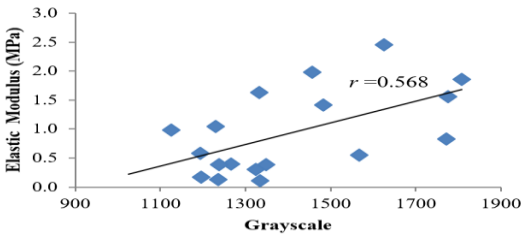

(a)

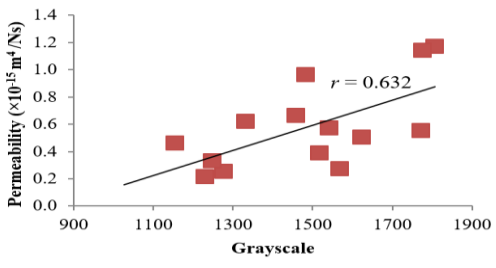

(b)

Fig. 8: Linear correlation between the MRI image grayscale and biomechanical properties of cartilage (a) elastic modulus (b) permeability.

4. Conclusion

This study presented the application of low-field MRI to examine the articular cartilage. Although there have been extensive studies to quantify the articular cartilage using high-field MRI unit, limited work has been carried out to examine the potential used of low-field MRI. The low-field MRI was able to provide grayscale values throughout the thickness of the cartilage. Furthermore, the correlation results between image grayscale from low-field MRI and the biomechanical properties of articular cartilage were observed to be in similar range to the previous studies using high-field MRI. These could indicate the potential application of low-field MRI to evaluate the biomechanical properties of articular cartilage. However, further studies are required to assess the low-field MRI on the biomechanical integrity of articular cartilage.

Acknowledgement

This study is funded by the Ministry of Science, Technology and Innovation (MOSTI) under Science Fund (06-01-14-SF0109 L00020). The support from the Universiti Teknikal Malaysia Melaka (UTeM) is gratefully acknowledged.

References

[1] Dam EB, Lillholm M, Marques J & Nielsen M (2015), Automatic Segmentation of High- and Low-Field Knee MRIs Using Knee Image Quantification with Data from the Osteoarthritis Initiative. *Journal of Medical Imaging* 2(2), 024001.

[2] Liess C, Lüsse S, Karger N, Heller M & Glüer CC (2002), Detection of Changes in Cartilage Water Content Using MRI T2-Mapping in Vivo. *Osteoarthritis and Cartilage* 10(12), 907–913.

[3] Teeple E, Jay GD, Elsaid KA & Fleming BC (2013), Animal Models of Osteoarthritis: Challenges of Model Selection and Analysis. *The AAPS Journal* 15(2), 438–446.

[4] Franz T, Hasler EM, Hagg R, Weiler C, Jakob RP & Mainil-Varlet P (2001), In Situ Compressive Stiffness, Biochemical Composition, and Structural Integrity of Articular Cartilage of the Human Knee Joint. *Osteoarthritis and Cartilage* 9(6), 582–592.

[5] Mow VC & Huiskes R (2005), Basic Orthopaedic Biomechanics and Mechano-Biology, Third Edit ed., Philadelphia: Lippincott Williams & Wilkins.

[6] Nieminen MT, Töyräs J, Laasanen MS, Silvennoinen J, Helminen HJ & Jurvelin JS (2004), Prediction of Biomechanical Properties of Articular Cartilage with Quantitative Magnetic Resonance Imaging. *Journal of Biomechanics* 37(3), 321–328.

[7] Hani AFM, Kumar D, Malik AS, Ahmad RMKR, Razak R & Kiflie A (2015), Non-Invasive and In Vivo Assessment of Osteoarthritic Articular Cartilage: A Review on MRI Investigations. *Rheumatology International* 35(1), 1–16.

[8] Julkunen P, Korhonen RK, Nissi MJ & Jurvelin JS (2008), Mechanical Characterization of Articular Cartilage by Combining Magnetic Resonance Imaging and Finite-Element Analysis—a Potential Functional Imaging Technique. *Physics in Medicine and Biology* 53(9), 2425–2438.

[9] Kladny B, Bail H, Swoboda B, Schiwy-Bochat H, Beyer WF & Weseloh G (1996), Cartilage Thickness Measurement in Magnetic Resonance Imaging. *Osteoarthritis and Cartilage* 4(3), 181–186.

[10] Nissi MJ, Rieppo J, Töyräs J, Laasanen MS, Kiviranta I, Nieminen MT & Jurvelin JS (2007) Estimation of Mechanical Properties of Articular Cartilage with MRI – dGEMRIC, T2 and T1 Imaging in Different Species with Variable Stages of Maturation. *Osteoarthritis and Cartilage* 15(10), 1141–1148.

[11] Folkesson J, Dam EB, Olsen OF, Pettersen PC & Christiansen C (2007), Segmenting Articular Cartilage Automatically Using a Voxel Classification Approach. *IEEE Transactions on Medical Imaging* 26(1), 106–115.

[12] Woertler K, Strothmann M, Tombach B & Reimer P (2000), Detection of Articular Cartilage Lesions: Experimental Evaluation of Low- and High-Field-Strength MR Imaging at 0.18 and 1.0 T. *Journal of Magnetic Resonance Imaging* 11(6), 678–685.

[13] Ghazinoor S, Crues JV & Crowley C (2007), Low-Field Musculoskeletal MRI. *Journal of Magnetic Resonance Imaging* 25(2), 234–244.
[14] Qazi AA, Folkesson J, Pettersen PC, Karsdal MA, Christiansen C & Dam EB (2007), Separation of Healthy and Early Osteoarthritis by Automatic Quantification of Cartilage Homogeneity. *Osteoarthritis and Cartilage* 15, 1199–1206.
[15] Dam EB, Folkesson J, Pettersen PC & Christiansen C (2007), Automatic Morphometric Cartilage Quantification in the Medial Tibial Plateau from MRI for Osteoarthritis Grading. *Osteoarthritis and Cartilage* 15(7), 808–818.
[16] Ejbjerg BJ (2005), Optimised, Low Cost, Low Field Dedicated Extremity MRI Is Highly Specific and Sensitive for Synovitis and Bone Erosions in Rheumatoid Arthritis Wrist and Finger Joints: Comparison with Conventional High Field MRI and Radiography. *Annals of the Rheumatic Diseases* 64(9), 1280–1287.
[17] Lu W, Yang J, Chen S, Zhu Y & Zhu C (2015), Abnormal Patella Height Based on Insall-Salvati Ratio and Its Correlation with Patellar Cartilage Lesions : An Extremity-Dedicated Low-Field Magnetic Resonance Imaging Analysis of 1703 Chinese Cases. *Scandinavian Journal of Surgery* 105(3), 197-203.
[18] Latif MJA, Jin Z & Wilcox RK (2012), Biomechanical Characterisation of Ovine Spinal Facet Joint Cartilage. *Journal of Biomechanics* 45(8), 1346–1352.
[19] Pawaskar SS, Fisher J & Jin Z (2010), Robust and General Method for Determining Surface Fluid Flow Boundary Conditions in Articular Cartilage Contact Mechanics Modeling. *Journal of Biomechanical Engineering* 132(3), 031001–1–8.
[20] Jaafar YL, Latif MJA, Hashim NH & Kadir MRA (2016), The Effects of Thickness on Biomechanical Behaviour of Articular Cartilage: A Finite Element Analysis. *ARPN Journal of Engineering and Applied Sciences* 11(8), 5331–5335.
[21] Qu C, Hirviniemi M, Tiitu V, Jurvelin JS, Toyras J & Lammi MJ (2014), Effects of Freeze-Thaw Cycle with and without Proteolysis Inhibitors and Cryopreservant on the Biochemical and Biomechanical Properties of Articular Cartilage. *Cartilage* 5(2), 97–106.
[22] Wansin Y, Latif MJA, Saad NM, Alhabshi SMI & Kadir MRA (2017), Characterization of Articular Cartilage Using Low-Field Magnetic Resonance Imaging Image. *Journal of Medical Imaging and Health Informatics* 7(6), 1149–1152.
[23] Nieminen MT, Toyras J, Laasanen, MS, Rieppo J, Silvennoinen J, Helminen HJ & Jurvelin JS (2001), MRI Quantitation of Proteoglycans Cartilage Stifness in Bovine Humeral Head. *Annual Meeting of the Orthopaedic Research Society*, 25–28.
[24] Taylor SD, Tsiridis E, Ingham E, Jin Z, Fisher J & Williams S (2011), Comparison of Human and Animal Femoral Head Chondral Properties and Geometries. *Journal of Engineering in Medicine* 226(1), 55–62.
[25] Appleyard RC, Ghosh P & Swain MV (1999), Biomechanical, Histological and Immunohistological Studies of Patellar Cartilage in an Ovine Model of Osteoarthritis Induced by Lateral Meniscectomy. *Osteoarthritis and Cartilage* 7(3), 281–294.
[26] Treppo S, Koepp H & Quan EC (2000), Comparison of Biomechanical and Biochemical Properties of Cartilage from Human Knee and Ankle Pairs. *Journal of Orthopaedic Research* 18(5), 739–748.
[27] Yao JQ & Seedhom BB (1993), Mechanical Conditioning of Articular Cartilage to Prevalent Stresses. *British Journal of Rheumatology* 32(11), 956–965.
[28] Bhosale AM & Richardson JB (2008) Articular Cartilage: Structure, Injuries and Review of Management. *British Medical Bulletin* 87(1), 77–95.
[29] Fox AJS, Bedi A & Rodeo SA (2009), The Basic Science of Articular Cartilage: Structure, Composition, and Function. *Sports Health* 1(6), 461– 468.
[30] Potter HG (2006), Magnetic Resonance Imaging of Articular Cartilage: Trauma, Degeneration, and Repair. *American Journal of Sports Medicine* 34(4), 661–677.
[31] Potter HG & Koff MF (2012), MR Imaging Tools to Assess Cartilage and Joint Structures. *HSS Journal* 8(1), 29–32.
[32] Wayne JS, Kraft KA, Shields KJ, Yin C, Owen JR & Disler DG (2003), MR Imaging of Normal and Matrix-Depleted Cartilage: Correlation with Biomechanical Function and Biochemical Composition. *Radiology* 228(2), 493–499.